J|A|C|S
ARTICLES
Published on Web 01/09/2007

Stabilization and Structure of Telomeric and c-myc Region Intramolecular G-Quadruplexes: The Role of Central Cations and Small Planar Ligands

Valérie Gabelica,*,† Erin Shammel Baker,‡ Marie-Paule Teulade-Fichou,§ Edwin De Pauw,† and Michael T. Bowers*,‡

Contribution from the Department of Chemistry, University of Liège, Belgium, the Department of Chemistry and Biochemistry, University of California at Santa Barbara, and the Collège de France, Paris, France

Received August 17, 2006; E-mail: v.gabelica@ulg.ac.be (V.G.); bowers@chem.ucsb.edu (M.T.B.)

Abstract: A promising approach for anticancer strategies is the stabilization of telomeric DNA into a G-quadruplex structure. To explore the intrinsic stabilization of folded G-quadruplexes, we combined electrospray ionization mass spectrometry, ion mobility spectrometry, and molecular modeling studies to study different DNA sequences known to form quadruplexes. Two telomeric DNA sequences of different lengths and two DNA sequences derived from the NHE III_1 region of the c-myc oncogene (Pu22 and Pu27) were studied. NH_4^+ and the ligands PIPER, TMPyP4, and the three quinacridines MMQ1, MMQ3, and BOQ1 were complexed with the DNA sequences to determine their effect on the stability of the G-quadruplexes. Our results demonstrate that G-quadruplex intramolecular folds are stabilized by NH_4^+ cations and the ligands listed. Furthermore, the ligands can be classified according to their ability to stabilize the quadruplexes and end stacking is shown to be the dominant mode for ligand attachment. In all cases our solvent-free experimental observations and theoretical modeling reveal structures that are highly relevant to the solution-phase structures.

Introduction

DNA sequences that are rich in guanines can form four-stranded structures called G-quadruplexes, which are stabilized by Hoogsteen hydrogen bonds between four guanines (known as a G-quartet).[1] G-rich sequences are significantly over-represented at several specific locations in the genome such as gene promoters[2−5] and introns,[6−8] and are therefore suspected of playing key roles in gene expression. G-rich sequences are also found in the telomeres, which are the nucleo-protein complexes at the end of the chromosomes that prevent chromosome ends from fraying or being recognized as DNA strand breaks.[9,10] The targeting of telomere maintenance processes is an attractive strategy in the design of anticancer therapeutics because one of the key properties of cancer cells is to circumvent telomere shortening processes that lead eventually to normal cell death (senescence).[11] Approximately 85% of cancer cells overexpress an enzyme called telomerase, a reverse transcriptase that binds to telomeric DNA and appends additional telomeric repeats, thereby elongating the telomeres. This process has the effect of making cancer cells immortal and allowing continual cell division without telomere shortening and subsequent senescence. One promising approach for altering the telomere structure and hence the association of telomeric DNA with its specific protein complexes is the stabilization of the telomeric DNA single-stranded G-rich overhang into a G-quadruplex structure.[12−14]

The screening of new ligands designed for stabilizing G-quadruplex structures is usually performed *in vitro* using functional assays (i.e., Telomeric Repeat Amplification Protocol (TRAP) assays, which probe telomerase inhibition), or binding assays (equilibrium dialysis,[15] fluorescence resonance energy transfer (FRET),[16] or mass spectrometry assays[17]). Good correlation has been demonstrated between binding and functional

† University of Liège.
‡ University of California at Santa Barbara.
§ Collège de France.

(1) Davis, J. T. *Angew. Chem., Int. Ed.* **2004**, *43*, 668.
(2) Dai, J.; Dexheimer, T. S.; Chen, D.; Carver, M.; Ambrus, A.; Jones, R. A.; Yang, D. *J. Am. Chem. Soc.* **2006**, *128*, 1096.
(3) De, A. R.; Wood, S.; Sun, D.; Hurley, L. H.; Ebbinghaus, S. W. *Biochemistry* **2005**, *44*, 16341.
(4) Rankin, S.; Reszka, A. P.; Huppert, J.; Zloh, M.; Parkinson, G. N.; Todd, A. K.; Ladame, S.; Balasubramanian, S.; Neidle, S. *J. Am. Chem. Soc.* **2005**, *127*, 10584.
(5) Siddiqui-Jain, A.; Grand, C. L.; Bearss, D. J.; Hurley, L. H. *Proc. Natl. Acad. Sci. U.S.A.* **2002**, *99*, 11593.
(6) Gomez, D.; Lemarteleur, T.; Lacroix, L.; Mailliet, P.; Mergny, J. L.; Riou, J. F. *Nucleic Acids Res.* **2004**, *32*, 371.
(7) Kostadinov, R.; Malhotra, N.; Viotti, M.; Shine, R.; D'Antonio, L.; Bagga, P. *Nucleic Acids Res.* **2006**, *34*, D119.
(8) Huppert, J. L.; Balasubramanian, S. *Nucleic Acids Res.* **2005**, *33*, 2908.
(9) Blasco, M. A. *Nat. Rev. Genet.* **2005**, *6*, 611.
(10) Blackburn, E. H. *FEBS Lett.* **2005**, *579*, 859.
(11) Hahn, W. C.; Counter, C. M.; Lundberg, A. S.; Beijersbergen, R. L.; Brooks, M. W.; Weinberg, R. A. *Nature* **1999**, *400*, 464.
(12) Riou, J.-F. *Curr. Med. Chem.* **2004**, *4*, 439.
(13) Hurley, L. H. *Nature Rev. Cancer* **2002**, *2*, 188.
(14) Neidle, S.; Parkinson, G. *Nature Rev. Drug Discov.* **2002**, *1*, 383.
(15) Ren, J.; Chaires, J. B. *Biochemistry* **1999**, 16067.
(16) Mergny, J.-L.; Lacroix, L.; Teulade-Fichou, M.-P.; Hounsou, C.; Guittat, L.; Hoarau, M.; Arimondo, P. B.; Vigneron, J.-P.; Lehn, J.-M.; Riou, J.-F.; Garestier, T.; Hélène, C. *Proc. Natl. Acad. Sci. USA* **2001**, *98*, 3062.
(17) Rosu, F.; De Pauw, E.; Guittat, L.; Alberti, P.; Lacroix, L.; Mailliet, P.; Riou, J.-F.; Mergny, J.-L. *Biochemistry* **2003**, *42*, 10361.

Scheme 1

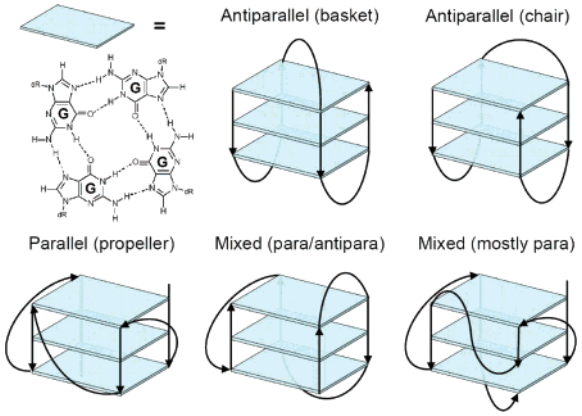

assays, thereby validating the G-quadruplex as a worthwhile target.[12−14,16] Consequently, in the last 5 years there has been a renewed interest in thermodynamic and structural studies on G-quadruplexes and their complexes with ligands. However, many challenges in studying G-quadruplex structures have occurred due to the numerous possible loop arrangements. X-ray and NMR structures of several intramolecular G-quadruplexes have been solved,[18−22] and some of the loop arrangements that were found are represented in Scheme 1. Several G-rich sequences, and notably the human telomeric sequence $(TTAGGG)_n$, have proven to be quite polymorphic.[20,23−25] Moreover, the structures adopted and their relative stabilities are influenced by the nature of the cations present in solution.[24−28] Some ligands can also displace the equilibrium between the different structures by specific binding to a certain loop arrangement.[29,30] Understanding cation and ligand-induced stabilization of particular G-quadruplex structures is therefore a cornerstone for the design of new specific ligands aimed at targeting a particular promoter or the telomeres. A problem is that interpretation of solution-phase data is complicated by the simultaneous presence of multiple stoichiometries (number of strands, number of cations, and/or number of ligands) and multiple conformations.

Electrospray mass spectrometry (ESI-MS) is able to identify different complexes based on their masses, and therefore allows the separation of different stoichiometries.[31−33] In the field of G-quadruplex studies, ESI-MS has been successfully used to determine strand stoichiometries,[34−37] ligand stoichiometries,[17,38−40] and ligand binding constants.[17,39] Furthermore, when ESI-MS is combined with ion mobility studies, which separate different conformations based on the ion drift time into a high-pressure cell,[41] different conformations can be resolved for each mass-to-charge ratio. The utility for analyzing biological molecules with ion mobility combined with mass spectrometry has been demonstrated with many different sizes of DNA complexes from mononucleotides[42] to whole duplexes[43] up to 30 base pairs. Recently, ESI-MS in conjunction with ion mobility measurements have demonstrated the conservation of G-quadruplex structures in isolated deoxyguanosine clusters,[44] in strands constituted from the human telomeric sequence $(TTAGGG)_n$,[45] and in complexes between G-quadruplexes and cyclo[*n*]pyrrole ligands.[46]

In the present work, we focus on G-quadruplex formation and conformational changes induced by cation binding, ligand binding, and changes in ion internal energy. The ligands chosen for this study (Scheme 2) are the two quinacridines MMQ1 and MMQ3 and the bis-quinacridine BOQ1, which are all known to be potent telomerase inhibitors.[16,47] The two well-studied ligands TMPyP4[48] and PIPER[49] were also analyzed for comparison. The G-quadruplex forming oligonucleotides chosen are derived from the human telomeric sequence (a 21-mer $\mathbf{T_{3.5}}$ and a 36-mer $\mathbf{T_6}$) and from the NHE III_1 region of the c-myc oncogene (a 22-mer **Pu22** and a 27-mer **Pu27**. The data presented here demonstrates that G-quadruplex intramolecular folds can be stabilized by cations and ligands, and maintain structural integrity even for highly charged ions in the absence of solvent. This intrinsic stabilization of the quadruplex mirrors the stabilization that is known to occur in solution. The most important implication of this experimental finding is that in the particular case of G-quadruplexes, solvent-free structures can confidently be used to model solution phase behavior. Molecular modeling can therefore be performed in the absence of solvent at much lower computational cost and give valuable results. Moreover, additional solvent-free experimental approaches permitted by ESI-MS (H/D exchange,[50] ion mobility,[51] electron

(18) Ambrus, A.; Chen, D.; Dai, J. X.; Jones, R. A.; Yang, D. Z. *Biochemistry* **2005**, *44*, 2048.
(19) Phan, A.-T.; Modi, Y. S.; Patel, D. J. *J. Am. Chem. Soc.* **2004**, *126*, 8710.
(20) Neidle, S.; Parkinson, G. N. *Curr. Opin. Struct. Biol.* **2003**, *13*, 275.
(21) Wang, Y.; Patel, D. J. *Structure* **1993**, *1*, 263.
(22) Parkinson, G. N.; Lee, M. P. H.; Neidle, S. *Nature* **2002**, *417*, 876.
(23) Ourliac-Garnier, I.; Elizondo-Riojas, M. A.; Redon, S.; Farrell, N. P.; Bombard, S. *Biochemistry* **2005**, *44*, 10620.
(24) Lee, J. Y.; Okumus, B.; Kim, D. S.; Ha, T. *Proc. Natl. Acad. Sci. U.S.A.* **2005**, *102*, 18938.
(25) Ying, L. M.; Green, J. J.; Li, H. T.; Klenerman, D.; Balasubramanian, S. *Proc. Natl. Acad. Sci. U.S.A.* **2003**, *100*, 14629.
(26) He, Y. J.; Neumann, R. D.; Panyutin, I. G. *Nucleic Acids Res.* **2004**, *32*, 5359.
(27) Li, J.; Correia, J. J.; Wang, L.; Trent, J. O.; Chaires, J. B. *Nucleic Acids Res.* **2005**, *33*, 4649.
(28) Ambrus, A.; Chen, D.; Dai, J.; Bialis, T.; Jones, R. A.; Yang, D. *Nucleic Acids Res.* **2006**, *34*, 2723.
(29) Seenisamy, J.; Rezler, E. M.; Powell, T. J.; Tye, D.; Gokhale, V.; Joshi, C. S.; Siddiqui-Jain, A.; Hurley, L. H. *J. Am. Chem. Soc.* **2004**, *126*, 8702.
(30) Rezler, E. M.; Seenisamy, J.; Bashyam, S.; Kim, M. Y.; White, E.; Wilson, W. D.; Hurley, L. H. *J. Am. Chem. Soc.* **2005**, *127*, 9439.
(31) Smith, R. D.; Bruce, J. E.; Wu, Q.; Lei, Q. P. *Chem. Soc. Rev.* **1997**, *26*, 191.
(32) Hofstadler, S. A.; Griffey, R. H. *Chem. Rev.* **2001**, *101*, 377.
(33) Daniel, J. M.; Friess, S. D.; Rajagopalan, S.; Wendt, S.; Zenobi, R. *Int. J. Mass Spectrom.* **2002**, *216*, 1.
(34) Goodlett, D. R.; Camp, D. G.; Hardin, C. C.; Corregan, M.; Smith, R. D. *Biol. Mass Spectrom.* **1993**, *22*, 181.
(35) Krishnan-Ghosh, Y.; Liu, D.; Balasubramanian, S. *J. Am. Chem. Soc.* **2004**, *126*, 11009.
(36) Rosu, F.; Gabelica, V.; Houssier, C.; Colson, P.; De Pauw, E. *Rapid Commun. Mass Spectrom.* **2002**, *16*, 1729.
(37) Datta, B.; Bier, M. E.; Roy, S.; Armitage, B. A. *J. Am. Chem. Soc.* **2005**, *127*, 4199.
(38) David, W. M.; Brodbelt, J.; Kerwin, S. M.; Thomas, P. W. *Anal. Chem.* **2002**, *74*, 2029.
(39) Carrasco, C.; Rosu, F.; Gabelica, V.; Houssier, C.; De Pauw, E.; Garbay-Jaureguiberry, C.; Roques, B.; Wilson, W. D.; Chaires, J. B.; Waring, M. J.; Bailly, C. *Chem. Bio. Chem.* **2002**, *3*, 100.
(40) Pothukuchy, A.; Mazzitelli, C. L.; Rodriguez, M. L.; Tuesuwan, B.; Salazar, M.; Brodbelt, J. S.; Kerwin, S. M. *Biochemistry* **2005**, *44*, 2163.
(41) Wyttenbach, T.; Bowers, M. T. *Modern Mass Spectrom.* **2003**, *225*, 207.
(42) Gidden, J.; Bowers, M. T. *J. Phys. Chem. B* **2003**, *107*, 12829.
(43) Baker, E. S.; Bowers, M. T. in preparation.
(44) Baker, E. S.; Bernstein, S. L.; Bowers, M. T. *J. Am. Soc. Mass Spectrom.* **2005**, *16*, 989.
(45) Baker, E. S.; Bernstein, S. L.; Gabelica, V.; De Pauw, E.; Bowers, M. T. *Int. J. Mass Spectrom.* **2006**, *253*, 225.
(46) Baker, E. S.; Lee, J. T.; Sessler, J. L.; Bowers, M. T. *J. Am. Chem. Soc.* **2006**, *128*, 2641.
(47) Teulade-Fichou, M.-P.; Carrasco, C.; Guittat, L.; Bailly, C.; Alberti, P.; Mergny, J.-L.; David, A.; Lehn, J.-M.; Wilson, W. D. *J. Am. Chem. Soc.* **2003**, *125*, 4732.
(48) Han, F. X.; Wheelhouse, R. T.; Hurley, L. H. *J. Am. Chem. Soc.* **1999**, *121*, 3561.
(49) Becker, H. C.; Nordén, B. *J. Am. Chem. Soc.* **1999**, *121*, 11947.
(50) Hemling, M. E.; Conboy, J. J.; Bean, M. F.; Mentzer, M.; Carr, S. A. *J. Am. Soc. Mass Spectrom.* **1994**, *5*, 434.
(51) Wyttenbach, T.; Bowers, M. T. *Modern Mass Spectrom.* **2003**, *225*, 207.

Scheme 2

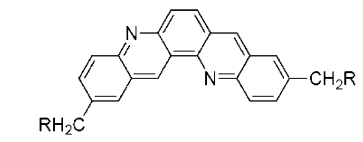

MMQ1, R = $NH(CH_2)_2CH_3$
MMQ3, R = $NH(CH_2)_3N(CH_3)_2$

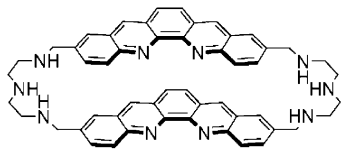

BOQ1

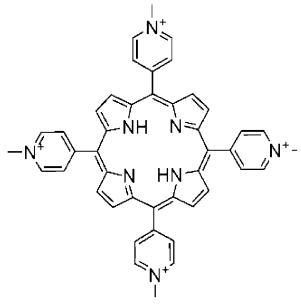

TMPyP4

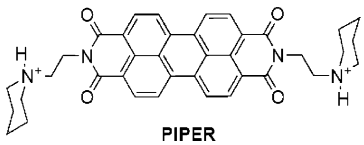

PIPER

capture or electron detachment dissociation[52] and spectroscopy[53]) might also be expected to give highly valuable structural information on G-quadruplex structures and their complexes.

Materials and Methods

Materials. DNA single strands were purchased from Eurogentec (Seraing, Belgium). Two strands containing the telomeric sequence (TTAGGG) with 3.5 and 6 repeats are named $\mathbf{T_{3.5}}$ [dGGG(TTAGGG)$_3$] and $\mathbf{T_6}$ [d(TTAGGG)$_6$], respectively. For the NHE III$_1$ region of the c-myc oncogene, two sequences were chosen with 22 and 27 bases, respectively. We will use the abbreviations **Pu22** for the 22 base strand dGAGGGTGGGGAGGGTGGGGAAG and **Pu27** for the 27 base strand dTGGGGAGGGTGGGGAGGGTGGGGAAGG. The ligands TMPyP4 and PIPER were purchased from Calbiochem (distributed by VWR International, Leuven, Belgium), whereas MMQ1, MMQ3, and BOQ1 were synthesized as described elsewhere.[54] All ligands were dissolved in water, except PIPER, which was dissolved in water acidified by 0.1% HOAc. The quadruplex 50 μM stock solutions were prepared in 100 mM NH_4OAc by annealing (heating at 80 °C followed by slow cooling). All solutions injected in nanoESI were 5 μM in quadruplex, 5 or 10 μM in ligand (depending on the apparent binding constants), 20 mM in NH_4OAc, and 20% methanol. Although rarely reported, previous control experiments with DNA−ligand combinations, which are known not to form any specific complex have proven that, when DNA and ligand concentrations are kept $\leq$10 μM, only specific complexes are observed.[55]

Mass Spectrometry and Ion Mobility Experiments. The instrument used for the ion mobility measurements has previously been described in detail.[56] Briefly, ions are generated by nanoESI and injected into an ion funnel through a 3-in long capillary, which was heated to 60−80 °C. The ion funnel essentially acts as an ion guide, compressing the stream of ions exiting the capillary and directing them toward the drift cell. The funnel is also used as an ion trap, allowing conversion of the continuous ion beam from the ESI source into a short ion pulse (1−5 μs) for the mobility measurements. The pulse of ions is injected into a 4.5-cm long drift cell containing ~5 Torr of helium gas. The voltage difference between the last lens and the drift cell is called the injection energy. This voltage is kept at 38 V for all determinations of collision cross sections. This value is the best compromise between ion transmission (too-low values result in a decrease of the signal) and ion activation due to collisions with helium out of the drift cell (too-high injection energies result in unfolding or fragmentation). An important diagnostic experiment can be done by varying the injection energy from the ion funnel into the drift cell. Injection at high-energy imparts internal energy into the system by collisional energy transfer. This transient pulse of energy is rapidly removed by subsequent collisions with the helium buffer gas. While energized, the system can isomerize or (if sufficiently energetic) dissociate. Injection at low energy best preserves the native conformations of the ions stored in the ion funnel.

In the drift cell, ions are quickly thermalized by collisions with the helium gas and drift through the cell under the influence of a weak, uniform electric field (10−23 V/cm). Collisions with the helium buffer gas broaden the injected ion packet and serve to bring a balance between the force imposed by the electric field and the frictional drag force. As a consequence, the ions drift at constant velocity, v_d, proportional to the applied field E;

$$v_d = KE \tag{1}$$

The proportionality constant, K, is termed the mobility. To obtain values independent of temperature T and pressure p, the reduced mobility K_o is usually determined:

$$K_o = \left(K \cdot \frac{p}{760} \cdot \frac{273.16}{T}\right) \tag{2}$$

Once K_o is determined, kinetic theory is applied to express K_o as a function of the collision system parameters:[57]

$$K_o = \frac{3q}{16N}\left(\frac{2\pi}{\mu k_b T}\right)^{1/2}\frac{1}{\sigma} \tag{3}$$

where q is the ion charge, N is the buffer gas density, μ is the reduced mass of the collision partners, k_b is Boltzmann's constant, and σ is the collision cross section.

As the ions exit the cell, they are mass analyzed with a quadrupole mass filter and detected as a function of time, yielding an arrival time distribution (ATD). Using eqs 1−3, it is straightforward to obtain an expression for the arrival time, t_A, in terms of the instrumental and molecular parameters:

$$t_A = \frac{l^2}{K_o} \cdot \frac{273.16}{760T} \cdot \frac{p}{V} + t_o \tag{4}$$

where l is the drift cell length, V is the voltage across the cell, and t_o is the time the ions spend outside the drift cell before detection. Hence, a plot of t_A versus p/V yields K_o from the slope and thus the cross

(52) Cooper, H. J.; Hakansson, K.; Marshall, A. G. *Mass Spectrom. Rev.* **2005**, *24*, 201.
(53) Oh, H. B.; Lin, C.; Hwang, H. Y.; Zhai, H.; Breuker, K.; Zabrouskov, V.; Carpenter, B. K.; McLafferty, F. W. *J. Am. Chem. Soc.* **2005**, *127*, 4076.
(54) Baudoin, O.; TeuladeFichou, M. P.; Vigneron, J. P.; Lehn, J. M. *J. Org. Chem.* **1997**, *62*, 5458.
(55) Rosu, F.; Pirotte, S.; De Pauw, E.; Gabelica, V. *Int. J. Mass Spectrom.* **2006**, *253*, 156.
(56) Wyttenbach, T.; Kemper, P. R.; Bowers, M. T. *Int. J. Mass Spectrom.* **2001**, *212*, 13.
(57) Masson, E. A.; McDaniel, E. W. *Transport Properties of Ions in Gases*; Wiley: New York, 1988.

section using eq 3. In a typical experiment, the pressure is held constant, while 5 different drift voltages are applied. The resultant plots are always linear with R^2 values greater than 0.9998.

Theoretical Calculations for Model Structures. Structural interpretation of the ATDs is performed by comparing the experimental cross sections to the cross sections of theoretical structures. Starting structures for theoretical analysis of the quadruplexes included the PDB structure 143D[21] (NMR structure of the human telomeric sequence $AGGG(TTAGGG)_3$ containing Na^+ ions) for the antiparallel quadruplexes, the PDB structure 1KF1[22] (crystal structure of the human telomeric sequence $AGGG(TTAGGG)_3$ with K^+ attached) for the parallel quadruplexes, and the PDB structure 186D[58] (NMR structure of the tetrahymena telomeric repeat $d(T_2G_4)_4$ for the mixed parallel/antiparallel quadruplexes. The molecular modeling program HyperChem (Hypercube Inc., 2002) was then used to make alterations to the loops of the different structures, so that the generated structures matched the sequences being analyzed. In the case of **Pu22**, the PDB structure 1XAV[18] was used without any modification with HyperChem since the PDB structure had the same sequence as the molecule analyzed in this study. Molecular dynamics simulations (300 K) were run on each structure for 2 ns using the AMBER 7 set of programs[59] and every 5 ps a structure was saved. Each structure was then energy minimized and its cross section calculated using hard-sphere scattering and trajectory models developed by the Jarrold group.[60,61] In these calculations, each starting structure eventually converges to give at least one steady-state structure where the cross section remains relatively constant. The average cross section of the final 50−100 structures in each steady state is then used for comparison with the experimental values.

The overall charge state of the quadruplexes can be readily identified from the mass spectra, but the exact locations of the deprotonation sites needed for the modeling are not known. Consequently, the same quadruplex structures were modeled with many different deprotonation sites. No significant differences in theoretical cross section or conformation were observed as a function of charge location, in agreement with modeling results published by Rueda et al.[62,63] To model the same total charge for quadruplexes with and without NH_4^+, one phosphate group is deprotonated for each additional NH_4^+ inserted between the quartets.

An annealing/energy minimization cycle was used to generate globular structures for each sequence. In this cycle, an initial minimization of the structure is followed by 30 ps of molecular dynamics at 600 K and 10 ps of molecular dynamics in which the temperature is incrementally dropped to 50 K. The resulting structure is then energy minimized again and used as the starting structure for the next minimization/dynamics run. After all low-energy structures are obtained, the theoretical cross sections are calculated. A scatter plot of cross section versus energy is collected for the minimized structures and the average cross section of the lowest 5−10 kcal/mol structures are then compared to the experiment.

Results and Discussion

1. Charge State Influences the Stability of Solvent-Free G-Quadruplexes. Oligonucleotides are naturally negatively charged in solution and spraying them produces a series of deprotonated species. A typical mass spectrum is given in Figure 1 for $\mathbf{T_6}$. Mass spectra for all species are given in the Supporting Information. Typically, a range of charge states is observed in the nanoESI mass spectra with the lower charge states being the dominant species. Each charge state is interrogated using ion mobility and structural information is obtained by comparison with molecular dynamics calculations. The arrival time distributions (ATDs) measured for the most intense charge states from the mass spectra are shown in Figure 2, together with the average experimental collision cross sections obtained from this data. The theoretical cross sections calculated for the lowest charge states of each quadruplex in different conformations are gathered in Table 1.

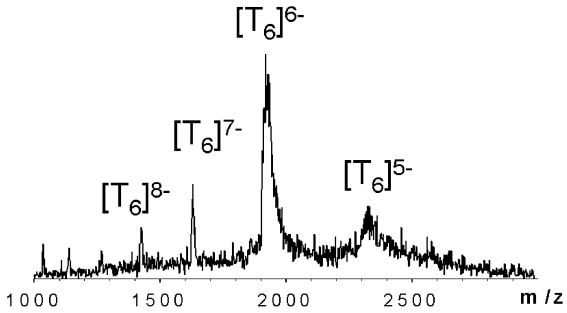

Figure 1. Typical mass spectrum obtained for $\mathbf{T_6}$.

For the small telomeric sequence $\mathbf{T_{3.5}}$, the two most intense charge states in the mass spectra are 4- and 5-. A 4% increase in the experimental cross section (from 688 to 718 $Å^2$) of $\mathbf{T_{3.5}}$ was observed as the charge state increased from 4− to 5−. When molecular modeling was performed an increase in cross section was also observed in the theoretical structures. This strand expansion is most probably due to an increase in Coulomb repulsion between the negative charge sites. By comparing the experimental and theoretical cross sections, the structure that best matches the experimental results for both charge states is the antiparallel structure. This is an unambiguous assignment due to the 90 $Å^2$ difference between parallel and antiparallel cross sections. This result provides very interesting information about the $\mathbf{T_{3.5}}$ sequence because it has been used previously as a screening agent for quadruplex-ligand specificity.[17,39,64,65] CD spectroscopy indicates that the antiparallel fold is predominant in ammonium acetate solution.[36] The present results therefore show that the solution G-quadruplex conformation is maintained following spraying, solvent evaporation, and ion mobility analysis.

The complete analysis of experimental and theoretical cross sections is reported elsewhere for $\mathbf{T_4}$ and $\mathbf{T_6}$.[45] However, to introduce how NH_4^+ ions and various ligands effect structure stability, the results of the $\mathbf{T_6}$ conformation assignments are briefly discussed here. The lowest charge states of $\mathbf{T_6}$, 5− and 6− both show single peak ATDs with cross sections around 1000 $Å^2$. To assign a structure to these cross sections, theoretical modeling was employed. However, the theoretical modeling of $\mathbf{T_6}$ was a little more difficult than $\mathbf{T_{3.5}}$, because it had to include several possibilities for placement of the two extra repeats in the quadruplex, i.e., in one of the loops or at the end of the DNA strand (Scheme 3). The comparison between experimental and theoretical cross sections indicates that the 5− and 6− charges states of $\mathbf{T_6}$ are antiparallel G-quadruplexes with the "extra" repeats on the ends. Charge state 7− for $\mathbf{T_6}$ is the critical

(58) Wang, Y.; Patel, D. J. *Structure* **1994**, *2*, 1141.
(59) Case, D. A. et al. *AMBER 7*; University of California: San Francisco, 2002.
(60) Shvartsburg, A. A.; Jarrold, M. F. *Chem. Phys. Lett.* **1996**, *261*, 86.
(61) Mesleh, M. F.; Hunter, J. M.; Shvartsburg, A. A.; Schatz, G. C.; Jarrold, M. F. *J. Phys. Chem.* **1996**, *100*, 16082.
(62) Rueda, M.; Kalko, S. G.; Luque, F. J.; Orozco, M. *J. Am. Chem. Soc.* **2003**, *125*, 8007.
(63) Rueda, M.; Luque, F. J.; Orozco, M. *J. Am. Chem. Soc.* **2006**, *128*, 3608.
(64) Guittat, L.; Alberti, P.; Rosu, F.; Van Miert, S.; Thetiot, E.; Pieters, L.; Gabelica, V.; De Pauw, E.; Ottaviani, A.; Riou, J.-F.; Mergny, J.-L. *Biochimie.* **2003**, *85*, 535.
(65) Guittat, L.; De Cian, A.; Rosu, F.; Gabelica, V.; De Pauw, E.; Delfourne, E.; Mergny, J. L. *Biochim. Biophys. Acta.* **2005**, *1724*, 375.

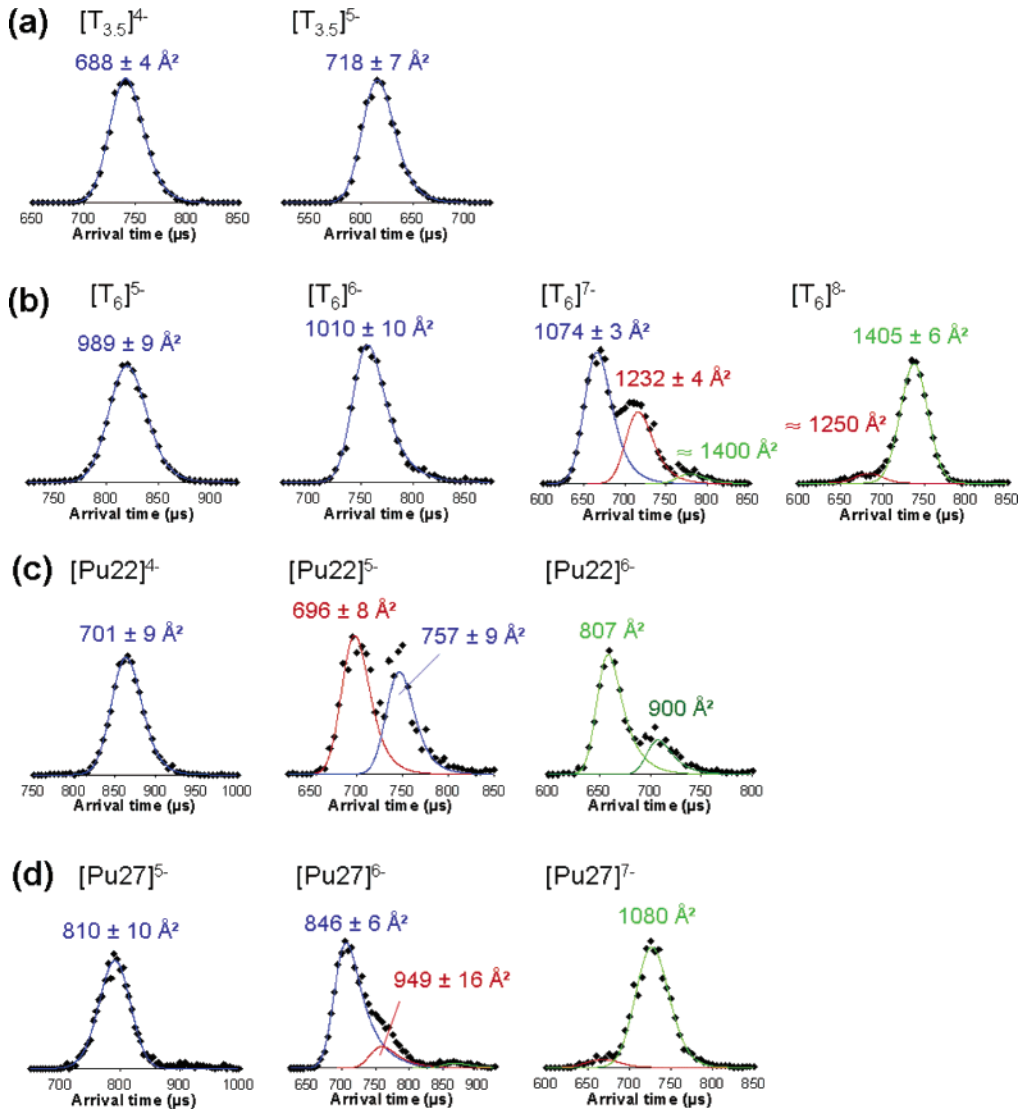

Figure 2. ATDs and experimental cross sections for the systems shown. Cross sections in blue correspond to conformations with the complete G-quadruplex intact (see text for the discussion of assignment), those in red correspond to the conformations with one G-quartet broken, and those in green correspond to further steps of G-quadruplex degradation.

charge state of transition from the folded G-quadruplex to a partially unfolded structure. MD simulations have shown that the peak with a cross section of 1074 Å^2 (Figure 2) corresponds to a nearly intact quadruplex (1 G-quartet broken) and the peak with the cross section of 1232 Å^2 corresponds to a structure with 2 G-quartets broken. The longest time peak (1400 Å^2) corresponds to an even more extended structure with all G-quartets broken.[45] The values of the cross sections do not depend on experimental conditions. The very sensitive 7− charge state was therefore studied in more detail as a function of cation and ligand binding (see sections 2 and 3). The collision cross section obtained for charge state 8− is 1400 Å^2, indicating a completely denatured structure.

In addition to the telomeric quadruplexes, we decided to study the two sequences **Pu22** and **Pu27**, which are known to form parallel G-quadruplexes in solution.[18,19] We performed CD experiments that confirmed that this is the case in ammonium acetate as well (data not shown). Moreover, it was reported that TMPyP4 could induce conformational changes in **Pu27**.[29] For **Pu27**, two sets of calculations were performed: one with the extra repeat in a loop and one with the extra repeat at the end of the strand (Scheme 3). The recent publication of the crystallographic structure of an analog structure *Pu24I*[66] indicated that a mixed mostly parallel structure could also exist (Scheme 1), so we also included this structure in our modeling.

In this section, only the lowest charge states will be discussed because they exhibit intact G-quadruplex structures. For **Pu22** and **Pu27** comparison between theoretical and experimental cross sections indicates that the best match is obtained for the parallel structure (with the extra repeats on the end of the strand for **Pu27**). An interesting observation is that both for the $\mathbf{T}_n$ and **Pu2X** sequences, the G-quadruplex conformation adopted is always the one with the smallest collision cross section, i.e., the most compact conformation. More experimental data with other sequences would be needed to assess whether it is a general rule that could be used to predict the adopted structure.[67] It is also generally observed that the structures found here are the same as those found by CD or NMR in solution, i.e.,

(66) Phan, A.-T.; Kuryavyi, V.; Gaw, H. Y.; Patel, D. J. *Nat. Chem. Biol.* **2005**, *1*, 167.
(67) Hazel, P.; Huppert, J.; Balasubramanian, S.; Neidle, S. *J. Am. Chem. Soc.* **2004**, *126*, 16405.

Table 1. Theoretical Cross Sections (Å^2) Calculated for Each G-Quadruplex for the Lowest Experimentally Observed Charge States

	$[T_{3.5}]^{4-}$	$[T_{3.5}]^{5-}$	$[T_6]^{5-}$ (ref 43)		$[Pu22]^{4-}$	$[Pu27]^{5-}$	
experimental	688	718	989		701	810	
theoretical			end	loop		end	loop
antiparallel (basket)	**700**	**713**	**1005**[b]	1060[c]	755	872	920
antiparallel (chair)	**700**	**712**	**1003**[d]	1065[e]	753	868	915
parallel (propeller)	790	802	1083	1092	**706**	**820**	907
mixed (para/antipara)	737	740	1047	1045	735	842	890
mixed (mostly para)	–	–	–	–	–	**818**	–
globular	660	662	1055	1049	743	856	858

[a]The different structures that were modeled are named according to Schemes 1 and 3. Reported cross sections are for quadruplexes without NH_4^+ ions complexed. Modeling with NH_4^+ located between G-quartet planes leads to nearly identical cross sections and structures. Cross sections in bold indicate those structures that best match the experimental values. [b] Values from 1003 to 1008 Å^2, depending on the placement of the extra G repeats (ref 43). [c] Values from 1040 to 1086 Å^2, depending on the placement of the extra G repeats (ref 43). [d] Values from 1002 to 1005 Å^2, depending on the placement of the extra G repeats (ref 43). [e] Values from 1045 to 1093 Å^2, depending on the placement of the extra G repeats (ref 43).

Table 2. Comparison of NMR/CD Solution Structures with Solvent-Free Structures

system	NMR/CD structure[a]	solvent-free structure[a,b]
$T_{3.5}$	antiparallel[21]	antiparallel
T_4	antiparallel[45]	antiparallel[45]
T_6	antiparallel[45]	antiparallel
Pu22	parallel[18]	parallel
Pu27	parallel[29]	parallel

[a] References for the solution structure assignments are noted in superscript. [b] This work.

Scheme 3

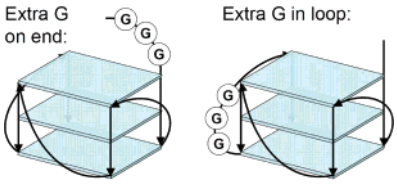

antiparallel for telomeric quadruplex[21,36] and parallel for **Pu2X** quadruplexes,[18,29] strongly supporting the idea of structure preservation during the spray and solvent evaporation process. Our results are summarized in Table 2.

2. The Role of Ammonium Cations on G-Quadruplex Stability. The lowest charge states of the G-quadruplexes, either with or without ammonium cations attached, have single-peaked ATDs with experimental cross sections in excellent agreement with the theoretical cross sections derived from the respective solution-phase structures. Clearly, attachment of ammonium cations is not essential for G-quadruplex stability either in solution or in a solvent-free environment. However, when the charge state increases, transition from a folded (quadruplex) to a denatured (broken quadruplex) conformation occurs. Some intermediate charge states displaying ATDs with several peaks are $[\mathbf{T_6}]^{7-}$, $[\mathbf{Pu22}]^{5-}$, and $[\mathbf{Pu27}]^{6-}$, as shown in Figure 2. For these charge states, it was observed that the preferred conformation depended on the number of attached NH_4^+ ions (0, 1, or 2). The influence of NH_4^+ on the ATDs is shown in Figure 3. For **Pu27** and $\mathbf{T_6}$, adding ammonium cations favors the most compact conformation, whereas for **Pu22** the reverse is observed. The result for **Pu22** seems surprising as native conformations are usually more compact than denatured ones. However, control experiments with varying injection energy also reveal that the shortest time peak (most compact conformation) is favored at low injection energy for **Pu27** and $\mathbf{T_6}$, whereas the longer time peak (most extended conformation) is favored at low injection energies for **Pu22**. It is expected that when ion internal energy (here governed by injection energy) or temperature is lower, or when central cations are retained between the quartets, the complex will tend to keep its initial (solution) conformation.[63] Because our injection energy results mirror those observed for sequential NH_4^+ addition shown in Figure 3, we deduce that the conformation of $[Pu22]^{5-}$ at longer times and the conformation of $[Pu27]^{6-}$ at shorter times are closest to the native conformation and hence are labeled as N in Figure 3.

Molecular dynamics simulations were run to interpret the evolution of the cross sections of $[\mathbf{Pu22}]^{5-}$ and $[\mathbf{Pu27}]^{6-}$ in terms of structure. The MD simulations were run for 2 ns, starting with the published NMR parallel structures (Figure 4). First, consider $[\mathbf{Pu22}]^{5-}$ with and without 2 NH_4^+ cations attached (Figure 4a and 4b). The simulation in Figure 4a begins with a structure similar to the solution NMR structure with all three quartets intact (N). After ~0.3 ns, it isomerizes to a more compact structure also with the G-quartets intact, but with a different side-chain orientation. This more compact distorted structure (D) is retained during the remaining simulation time. However, when two stabilizing NH_4^+ ions are added (Figure 4b), the structure retains the (NMR-like) solution structure (N) for the entire simulation time. A somewhat different picture arises for the larger $[\mathbf{Pu27}]^{6-}$ system. Here, the system retains the pseudo NMR solution structure (N) for ~1.25 ns (Figure 4c) with all G-quartets intact before isomerizing to a larger structure with one G-quartet broken (D). When two NH_4^+ ions are added (Figure 4d), the system retains the (NMR-like) solution structure (N) throughout the simulation.

The cross sections shown for the various structures in the MD simulations in Figure 4 quantitatively correlate with the similarly labeled features in the ATDs in Figure 3. In the case of the telomeric quadruplex $\mathbf{T_6}$, the antiparallel conformation of $[\mathbf{T_6}]^{7-}$ qualitatively behaves like $[\mathbf{Pu27}]^{6-}$, with G-quartets breaking at longer simulation times resulting in an increase of collision cross section, as shown elsewhere.[45] In summary, we have demonstrated that for these two very important families of G-quadruplexes (telomeric and **Pu2X**), low charge states maintain their structure in the absence of solvent without central cations. However, ammonium cations play a crucial role in preserving the solution-phase conformation of G-quadruplexes in medium to high charge states. In no instance did we observe changes in basic quadruplex conformation as ammonium ions are added to the quadruplex, i.e., parallel did not go to antiparallel upon the addition of NH_4^+.

3. Bound Ligands Increase the Stability of G-Quadruplexes. As noted in the introduction, there currently is intense interest in finding suitable, nontoxic ligands that can stabilize G-quadruplexes. Here we investigate a series of ligands and a series of quadruplexes to pursue this goal by characterizing ligand-induced increases of quadruplex stability or possible ligand-induced structural changes. Five ligands of interest are

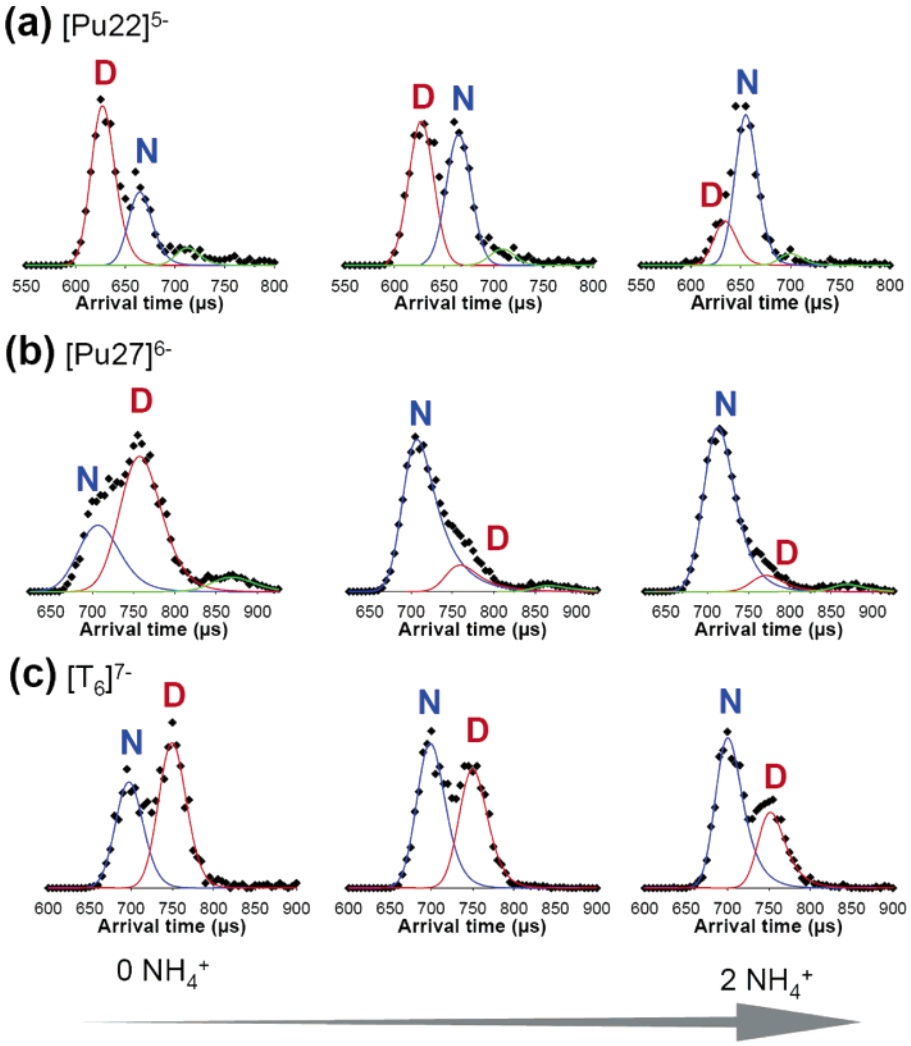

Figure 3. Influence of the presence of NH_4^+ on the ATDs of (a) $[Pu22]^{5-}$, (b) $[Pu27]^{6-}$, and (c) $[T_6]^{7-}$ at fixed injection energy and drift voltage. The labels on the peaks indicate native-like structure (N) or distorted structure (D), in agreement with simulations given in Figure 4.

shown in Scheme 2. Solutions of these ligands were made with each of the quadruplexes discussed above and cross sections were measured for all 20 systems. These cross sections can be compared with calculations to determine both the structure of the quadruplex and the ligand-quadruplex complex. The majority of this data is placed in Supporting Information with key results summarized here.

When systems with intact G-quadruplex structures are complexed with ligands, the initial G-quadruplex structure is universally retained (antiparallel for $\mathbf{T}_n$ sequences and parallel or mostly parallel for **Pu2X** sequences). In all cases, modeling indicates that the ligand either externally stacks or intercalates. Nonspecific binding gives collision cross sections that are too large compared to the experimental values. Table 3 gives the data for the complexes with $[\mathbf{T_{3.5}}]^{5-}$ and $[\mathbf{Pu22}]^{5-}$. End stacking and intercalating binding modes cannot be distinguished based on the cross sections except in the case of BOQ1, for which the intercalated complex is significantly larger than the end stacked complex. The experimental cross section therefore unambiguously indicates that end stacking is the binding mode for BOQ1. The structures of the complexes with $\mathbf{T_{3.5}}$ are shown in Figure 5, and those with **Pu22** in Supporting Information. Calculations indicate that in all cases end stacked structures are at least 20 kcal/mol lower in energy than the intercalated structures. This finding is also compatible with the conservation of 2 ammonium ions when those quadruplex systems attach a ligand. Intercalation would result in the loss of an ammonium ion, but this is not observed. Hence, our mass spectrometry, ion mobility, and modeling data indicate that end stacking is the dominant binding mode for the ligands and DNA sequences studied.

To probe the extent to which ligand end-stacking stabilizes the G-quadruplex, we examined the critical charge states $[\mathbf{T_6}]^{7-}$, $[\mathbf{Pu22}]^{5-}$, and $[\mathbf{Pu27}]^{6-}$ more closely, in the absence and presence of ligand. The $[\mathbf{Pu22}]^{5-}$ system exhibits only a parallel structure with the G-quadruplex intact. On the other hand, both $[\mathbf{T_6}]^{7-}$ and $[\mathbf{Pu27}]^{6-}$ are mixtures of conformers, one with the G-quadruplex intact and one with a broken G-quartet. The results obtained for the complex $[\mathbf{Pu27} + \text{TMPyP4}]^{6-}$ are described in the Supporting Information. We will focus here on the complexes with the telomeric G-quadruplex $[\mathbf{T_6}]^{7-}$, given the importance of telomeric G-quadruplex DNA as an antitumor drug target.

For the charge states that show transition from stable quadruplex structures to structures with broken quartets, the relative proportions of native and denatured conformations in the ATD spectra can depend on the spray conditions (see full discussion in Supporting Information). Therefore, in these

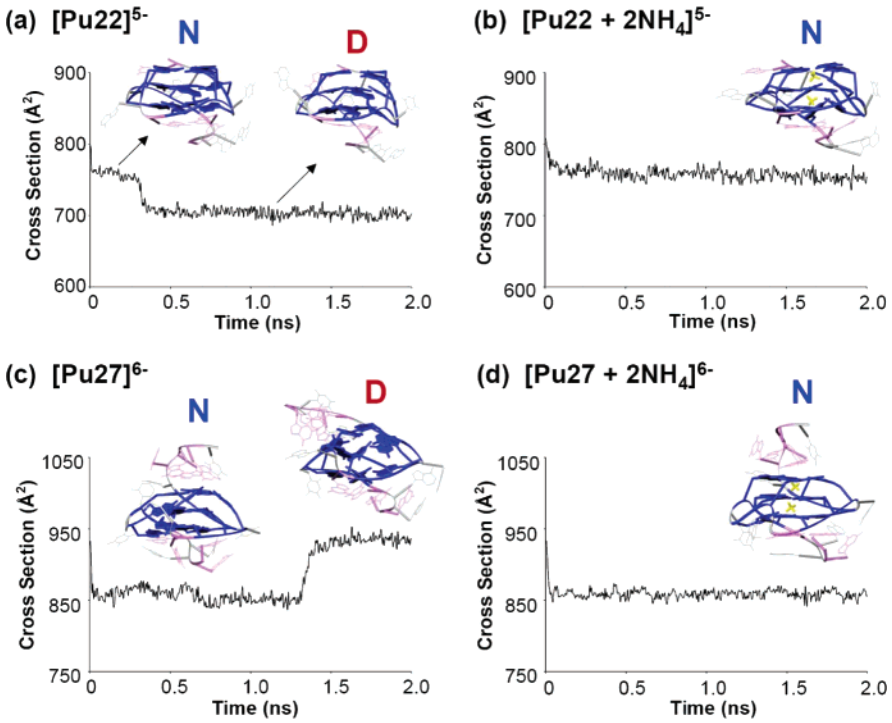

Figure 4. Modeling for the intermediate charge states of the myc G-quadruplexes in fully parallel conformation: comparison with and without NH_4^+. (a) [**Pu22**]$^{5-}$; (b) [**Pu22** + 2NH_4^+]$^{5-}$; (c) [**Pu27**]$^{6-}$; (d) [**Pu27** + 2NH_4^+]$^{6-}$. The labels (N for native-like, D for distorted) given for the various features correlate with the labels on the ATDs in Figure 3. The modeling of **Pu27** in the mostly parallel conformation is provided as Supporting Information (Figure S2).

Table 3. Experimental and Theoretical Cross Sections (Å^2) for the 1:1 Complexes between $\mathbf{T_{3.5}}$ and **Pu22** and the Five Different Ligands[a]

	[$\mathbf{T_{3.5}}$ + 1 Ligand]$^{5-}$				[**Pu22** + 1 Ligand]$^{5-}$			
	experimental	modeling end stack	modeling intercalated	modeling nonspecific	experimental	modeling end stack	modeling intercalated	modeling nonspecific
MMQ1	760 ± 6	765	763	785	780 ± 1	779	785	792
MMQ3	752 ± 2	766	765	791	767 ± 5	777	782	793
BOQ1	794 ± 0	789	815	817	773 ± 1	786	801	809
TMPyP4	750 ± 2	754	757	781	746 ± 12	760	764	783
PIPER	755 ± 3	759	760	787	761.5 ± 1	765	776	789

[a] Modeling data are reported here for $\mathbf{T_{3.5}}$ in an antiparallel conformation, and for **Pu22** in a parallel conformation. A full set of modeling data (with other quadruplex conformations) are provided in the Supporting Information.

comparisons between systems with and without ligands, we recorded the ATD spectra one after the other with the same needle. Consequently, the ATDs are slightly different from those shown in Figures 2 and 3. The data are shown in Figure 6 for the complexes of [$\mathbf{T_6}$]$^{7-}$ with 0, 1, and 2 ligands (MMQ1, MMQ3, and TMPyP4). The data clearly shows that the addition of a ligand stabilizes the conformation with an intact G-quadruplex. It is apparent that one MMQ1 is less effective than one MMQ3 or one TMPyP4 at stabilizing the quadruplex, but the addition of a second MMQ1 ligand further stabilizes the quadruplex conformation. The same effect was observed with the ligand PIPER (Figure 7, top spectra at 40 V). We can therefore classify the ligands according to their ability to stabilize the telomeric G-quadruplex: MMQ3 ≈ TMPyP4 > MMQ1 ≈ PIPER. The complex of $\mathbf{T_6}$ with BOQ1 was not intense enough at charge state 7- to allow reliable recording of its ATD.

The case of **Pu27** complexing with TMPyP4 is interesting because it has been reported that TMPyP4 induces a conformational transition from a parallel to an antiparallel structure in solution.[29,30] We have modeled this system in detail for [**Pu27**]$^{5-}$ with the complete results given in Supporting Information. For [**Pu27** + TMPyP4]$^{5-}$, the experimental cross section

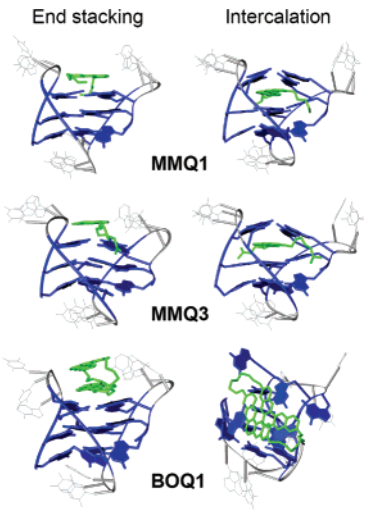

Figure 5. Structures for the end stacking and intercalated complexes between the G-quadruplex $\mathbf{T_{3.5}}$ and the ligands MMQ1 (top), MMQ3 (middle) and BOQ1 (bottom).

is 841 Å^2, in excellent agreement with a parallel end stacked or intercalated complex (the mixed, mostly parallel conformer

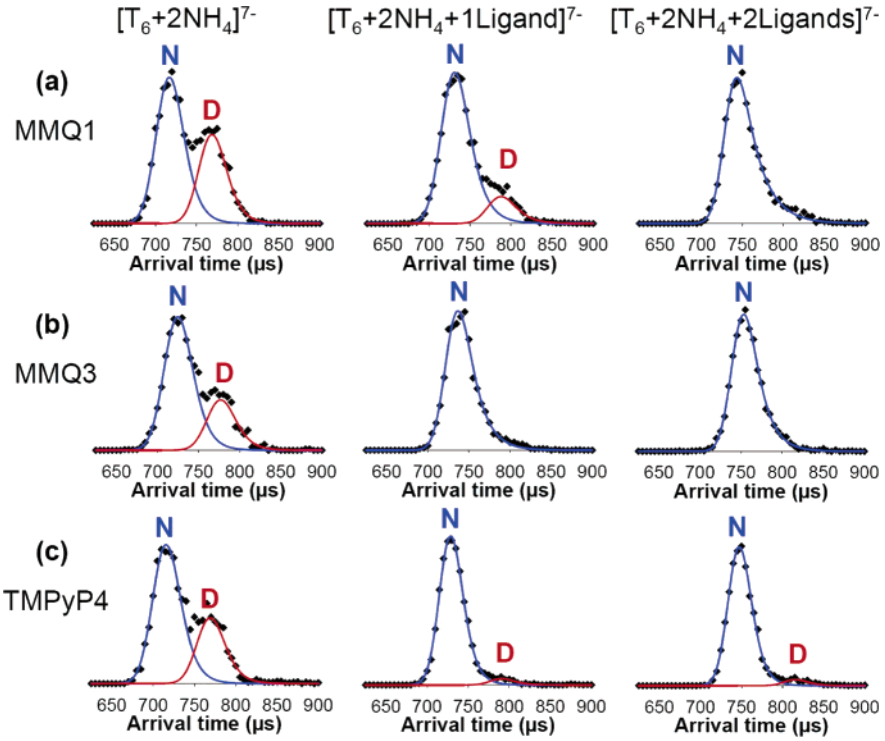

Figure 6. ATDs of $[\mathbf{T_6} + 2\ NH_4]^{7-}$ in the absence of ligand (left), with one ligand bound (middle), or two ligands bound (right): (a) MMQ1, (b) MMQ3, (c) TMPyP4. The injection energy was 40 V for all systems.

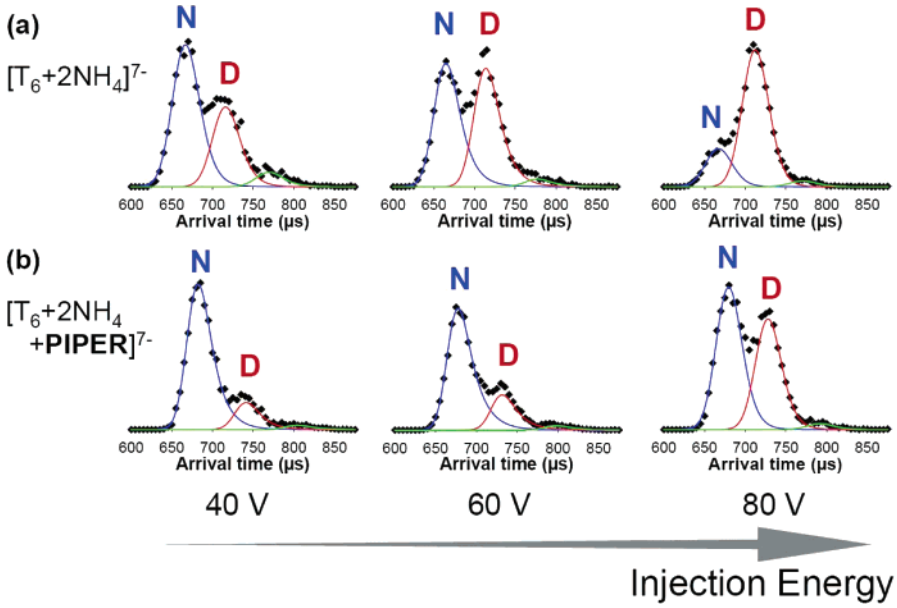

Figure 7. ATDs of $[\mathbf{T_6} + 2NH_4]^{7-}$ (a) in the absence of ligand and (b) in the presence of PIPER, as a function of the injection energy voltage (40, 60, and 80 V).

is only a small amount too large). However, the antiparallel conformation is about 50 Å^2 too large and is clearly not observed in our experiment. There is no evidence for any system rearranging upon spraying and solvent evaporation with or without a ligand attached, and it is not expected that the [**Pu27** + TMPyP4]$^{5-}$ system would have done so (it would have to completely unfold and refold). The solution experiments[29] were done in the absence of buffer whereas our solutions were between 20 and 150 mM ammonium acetate. The origin of this discrepancy is not understood.

An interesting question concerns quadruplex stability in solvent-free conditions. We showed earlier that addition of NH_4^+ between G-quartet planes helped stabilize the quadruplex structures. It is clear that ligand attachment has at least as great a favorable effect on quadruplex stability. A qualitative indication of stability can be obtained from injection energy experiments. A set of ATDs at different injection energies is shown in Figure 7 for $[\mathbf{T_6} + 2NH_4 + \text{PIPER}]^{7-}$. The peak at short times is the intact quadruplex and the one at longer times is the conformation with one quartet broken. The $[\mathbf{T_6} + 2NH_4]^{7-}$

complex efficiently breaks one quartet as injection energy increases. The same effect occurs with PIPER complexed to $\mathbf{T_6}$ but much less efficiently, indicating the stabilizing influence of the ligand even in the presence of NH_4^+ cations. To obtain more quantitative thermodynamic parameters, conformational stability should be evaluated as a function of temperature. These experiments are difficult and, if successful, will be reported elsewhere.

Summary

The major findings of the work presented here are as follows.

1. For all nucleotide sequences studied, the desolvated systems retained the same folding as the G-quadruplex structures present in the spray solutions.

2. Increasing the charge state of desolvated structures leads to G-quartet breaking and eventually total denaturation of the quadruplex structure. The larger the system the higher the charge state must be to initiate denaturation.

3. Ammonium ions located between G-quartet planes stabilize quadruplex structures, and this stabilization is crucial to extend the range of charge states that can retain the solution-phase structure.

4. All ligands studied here stabilize the quadruplex structure. Even when NH_4^+ ions are complexed, additional stabilization is provided by the ligand. We find the following order of stability: MMQ3 $\approx$ TMPyP4 $>$ MMQ1 $\approx$ PIPER.

5. Although intercalation cannot be completely ruled out (except for BOQ1), end stacking appears to be the dominant mode for ligand binding.

6. The unambiguous retention of quadruplex structure for low charge states following electrospray and desolvation indicates other techniques using ESI can be applied to characterize these systems, including the complexes with ligands. Care must be taken not to energize the systems either during ion formation or analysis, however, or quadruplex denaturation will occur.

Acknowledgment. The support of the National Science Foundation under grant CHE-0503728 is gratefully acknowledged. V.G. is a Research Associate of the FNRS (Belgium), which is acknowledged for funding a research stay at UCSB.

Supporting Information Available: Full list of authors for reference 59, detailed discussion of the full scan electrospray mass spectra, 2 ns modeling of Pu27 in the mixed (mostly parallel) conformation, and determination of the ligand binding mode (including the full tables of experimental and theoretical cross sections). This material is available free of charge via the Internet at http://pubs.acs.org.

JA065989P